physica status solidi
pss
www.pss-journals.com

reprint

WILEY-VCH

Phys. Status Solidi B **248**, No. 1, 158–166 (2011) / **DOI** 10.1002/pssb.201083974

physica status solidi b
www.pss-b.com
basic solid state physics

Viscoelastic, dielectric, and thermal properties of $BaTiO_3$-3%$KNbO_3$

Liang Dong[1], Donald S. Stone[1], and Roderic S. Lakes*[,1,2,3]

[1] Materials Science Program, University of Wisconsin, Madison, WI 53706-1687, USA
[2] Department of Engineering Physics, University of Wisconsin, Madison, WI 53706-1687, USA
[3] Biomedical Engineering Department and Rheology Research Center, University of Wisconsin, Madison, WI 53706-1687, USA

Received 18 February 2010, revised 14 June 2010, accepted 17 June 2010
Published online 13 August 2010

Keywords 3%$KNbO_3$-$BaTiO_3$, viscoelastic, dielectric, core-shell structure, defect configuration

* Corresponding author: e-mail lakes@engr.wisc.edu, Phone: 608-265-8697, Fax: 608-263-7451

Viscoelastic behavior (modulus and damping) of polycrystalline 3%$KNbO_3$-$BaTiO_3$ has been studied in torsion and bending via broadband viscoelastic spectroscopy (BVS) over a range of temperature passing through both the orthorhombic-to-tetragonal and tetragonal-to-cubic phase transformations. Softening in bulk modulus and minima in Poisson's ratio as well as peaks in mechanical damping, dielectric constant, and heat capacity vs. temperature were observed in the vicinity of the transformations. Viscoelastic response vs. temperature was sharper than dielectric or thermal response. Transition temperatures of both transformations shifted to lower temperatures in comparison to pure $BaTiO_3$. Damping peaks vs. temperature were wider (5 °C) than in pure $BaTiO_3$ (less than 1 °C) and of smaller magnitude. Broadening of response is attributed to material heterogeneity on a fine scale.

1 Introduction Phase transformations in ferroelectric materials are of interest in several settings: as piezoelectric transducers, as capacitors, and as constituents in composites. Ferroelectric ceramics, when polarized, have piezoelectric properties useful in transducers. The piezoelectric properties vanish above the Curie temperature at which the crystals change to a form with too high symmetry to allow piezoelectricity. Therefore the Curie point must be well above any operating temperature. Barium titanate is a ferroelectric once commonly used as a transducer material, now supplanted by lead titanate zirconate ceramics which provide greater sensitivity. Because lead is toxic and presents environmental concerns, there is interest in lead free piezoelectric materials [1]. To that end, barium titanate doped with various constituents has been studied. The temperature for transformation to various crystal forms is altered by the doping. Although reduction in the Curie point by doping may be problematical for high temperature applications, the improvement in properties near ambient temperature is beneficial in the many applications of piezoelectric materials in which temperature is moderate.

Tuning of the transformation is also of interest in the context of composites based on negative stiffness. Landau's theory [2], which is generally considered as a phenomenological theory of phase transition, may be helpful in predicting negative elastic modulus (stiffness), as follows. In Landau's theory the free energy of the crystal is a function of both strain and temperature. At high temperature a single energy well is formed as a function of strain but as temperature is lowered the well gradually flattens, and develops two minima or potential wells. Therefore, the flattening of this curve represents the softening of the specific elastic modulus, and the reversed curvature below the transition temperature corresponds to a negative stiffness. Such a negative stiffness behavior during phase transformation in barium titanate ceramic has been inferred from the mechanical anomaly observed in particular composite materials of barium titanate ceramic in tin [3]. Softening of bulk modulus and negative Poisson's ratio have been experimentally observed in pure barium titanate ceramic in the vicinity of the Curie point (126 °C)[4]. Negative stiffness can be utilized to achieve extreme values of physical properties, and this was indeed achieved experimentally in the composite materials containing negative stiffness elements [3, 5]. However, application of such composite materials is restricted by the narrow and specified active

temperature regions. For example, $BaTiO_3$ has three first order transformations, which locate specifically at -80, 5, and 125 °C, respectively.

The Curie point of $BaTiO_3$ shifts to lower temperature by introducing certain kind of dopant, such as $KNbO_3$, $BaZrO_3$, $BaSnO_3$, etc (a phase diagram of the $KNbO_3$-$BaTiO_3$ system [6] is shown in Fig. 3). In this way, one can tune the transformation temperature by varying the amount of dopant, and hence enable the manipulation of negative stiffness behavior in the temperature domain. Transformation of doped $BaTiO_3$ should also be consistent with Landau's theory because the doped material still undergoes the same sort of phase transformation; moreover, there are no new parameters introduced into the Laudau free energy. To study this, it is necessary to experimentally measure the mechanical behaviors in the vicinity of tuned transformation temperature(s). In this study, viscoelastic properties of 3%$KNbO_3$-$BaTiO_3$ have been determined in torsion and bending via BVS in the temperature domain passing through both the orthorhombic-to-tetragonal (O-T) and tetragonal-to-cubic (T-C) transformations at subresonant frequencies. Moreover X-ray diffraction, dielectric, and differential scanning calorimetry (DSC) experiments were performed. The results are pertinent to tunable transformations for sensor and actuator materials and could be helpful for future research on particular composite materials containing negative stiffness elements with tunable activation temperatures.

2 Experimental method The ceramic was synthesized by means of solid state reaction. The procedure is based on the method outlined by Avrahami [1]. $KNbO_3$ (Alfa Aesar, 99.999% metal basis) and $BaTiO_3$ (Alfa Aesar, 99.7% metal basis) powders were used as precursors. Powders with desired molar ratio were mixed and ball milled in a silicon nitride vial for 2 h with a high energy milling machine (SPEX SamplePrep 8000-series Mill/Mixer). 3644 Ultrabind binder (SPEX CertiPrep PrepAid™) 10% by weight to sample was then added into the vial, and mixed for another 3 min to allow binder to evenly spread amid in the precursor powders. Powders were then transferred into a specially designed stainless steel compression mould with diameter of 25 mm, and a uniaxial pressure up to 150 MPa was applied using a hydraulic press (Carver Hydraulic) of capacity of 24 000 lbs at room temperature. The green pellet with typical dimensions ∅25 mm × 10 mm was taken out of the mould and solid state reacted and sintered (at atmospheric pressure) in air. Solid state reaction was performed in air at 750 °C for 4 h, followed by sintering in air at 1280 °C for 15 h. A ramp up rate of 3 °C/min was applied. Each sample was then cooled to ambient temperature with a rate of 4 °C/min. Samples were kept inside an alumina crucible with an alumina lid on top so as to avoid possible contamination from any residue left inside the furnace. To avoid reaction between sample and the crucible, samples were buried inside pure $BaTiO_3$ powders. To facilitate composition homogeneity, another two sintering steps were performed in sequence after the first sintering: the pellet was crushed, ground with a high density alumina mortar and pestle, and ball milled again for the same amount of time. Powders were uniaxially cold pressed into a pellet of dimensions ∅25 mm × 10 mm at 150 MPa and sintered in air at 1325 °C for 15 h. Before reaching the final sintering temperature, the pellet was held at 750 °C for 2 h to allow complete binder burning off. The same ramp up and ramp down rates as the first sintering step were applied. The final ceramic is light yellow in color. Too fast a ramping down rate will result in a dark gray color, a sign of reduction. A sintering temperature lower than 1200 °C is not appropriate as surface diffusion, rather than volume diffusion, will dominate and densification will not occur. To obtain higher density samples, hot press sintering can be used: the sample is kept inside a graphite mould, and one applies heat and pressure simultaneously during sintering. This method was not used in the present study.

Phase purity and unit-cell parameters determination have been performed via standard powder X-ray diffraction (Scintag PAD V XRD) for the doped $BaTiO_3$. As for comparison, the X-ray diffraction spectrum of the pure (undoped) $BaTiO_3$ has also been measured. During cooling, the crystalline symmetry decreases, and leads to the splitting of degenerate cubic diffraction peaks. For the tetragonal phase, the {100} peaks split into (100) and (001); for the orthorhombic phase, the {100} peaks split into (100), (010), and (001).

DSC tests were performed to determine the phase transition temperature. Both pure and doped $BaTiO_3$ were tested from −80 to 150 °C. A rate of 20 °C/min was applied. A specimen of mass 6 mg with thickness about 0.5 mm was used.

Reflection optical microscopy observation (Nikon Eclipse 80i light microscope with Nikon DXM1200F digital camera, Japan) was performed on a piece mechanically ground with SiC abrasive papers from 200 grit down to 1200 grit and finally polished with Al_2O_3 powders (0.3 μm) on a nap cloth. The specimen was etched for 3 min with etchant made of 100 ml of 10% HCl with several droplets of 48% HF [7] before observation.

Dielectric measurements have been performed on a piece (3%$KNbO_3$-$BaTiO_3$) with rectangular cross-section 9.3 mm × 5.9 mm, and a thickness of 1.58 mm over the temperature range of interest, −20 to 100 °C at several frequencies (10^3, 10^4, 10^5 Hz). A simple bridge circuit was used with the specimen in series with a capacitor of 1000 pF. A lock-in amplifier (Stanford Research System SR850) was used as both function generator and signal receiver. A thermal rate of 0.01 °C/s was maintained during the measurements. Temperature was monitored by a thermocouple (OMEGA L-0044 K type) 1 mm away from the specimen surface.

BVS has been used to study the mechanical loss and moduli in torsion and bending of the specimen over a temperature range –10 to 80 °C. The specimen was cut with a diamond saw to a size of 1.08 mm × 1.56 mm × 16.5 mm. Gold was sputtered onto all sample surfaces to achieve a near

electrical short-circuit boundary condition. The ceramic was not subjected to electric polarization (poling). Deformation of the specimen was induced by torque applied on the permanent magnet, and measured by a laser light reflected from a mirror mounted on the magnet to a wide-angle, two-axis photodiode position sensor (Pacific Silicon Sensor Inc. DL100-7PCBA, Westlake, CA). Data were captured by a lock-in amplifier (Stanford Research System SR850). Temperature was controlled via electrical input to resistance heaters which warmed a suitable amount of flowing air directed into the apparatus. The air flow subsequently served to heat up the specimen. Low temperature was achieved with the aid of the cooling module FLEXI COOLING system (FTS Systems Inc., Stone Ridge, NY). Temperature was monitored by a thermocouple (OMEGA L-0044 K type) 1 mm away from the sample surface at the base. Thermal gradient along the sample can be minimized within 0.2 °C.

3 Results

3.1 Optical microscopy An average grain size of 15 μm was observed; the grains were equiaxed which suggests isotropy. The smallest domain size observed via optical microscopy is about 1 μm (Fig. 1). A mass density of 5.38 g/cm^3 was determined from measured mass and dimensions, which is about 90% theoretical density (5.96 g/cm^3).

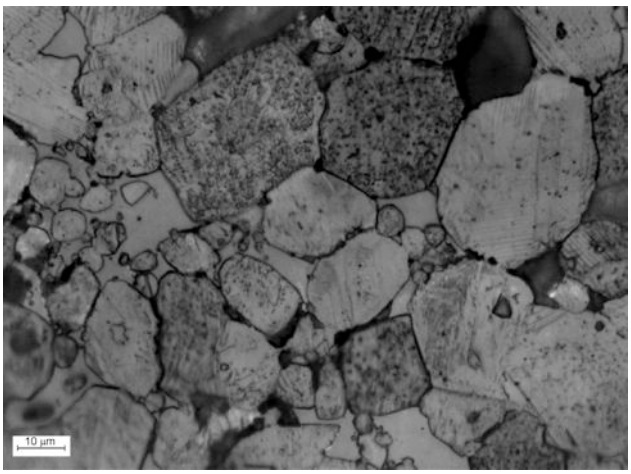

Figure 1 Microstructure of 3%$KNbO_3$-$BaTiO_3$ by means of reflection optical microscopy in polarized light (25 °C). The scale mark is 10 μm.

3.2 XRD Figure 2 presents the X-ray diffraction spectra of the doped and undoped $BaTiO_3$ at room temperature. The splitting of the {100} peak in the pure $BaTiO_3$ XRD spectrum is obvious, which indicates a tetragonal phase. The splitting of the {100} peak in the doped $BaTiO_3$ is not easy to be distinguished, however, the unsymmetrical characteristic of the {100} peak is detectable, which indicates either a tetragonal phase or an orthorhombic phase, or a coexistence of both phases. Since the optical microscopy observation reveals the presence of domains, it is safe to say the doped $BaTiO_3$ is in ferroelectric phase. XRD results did not reveal the presence of any minor phases, indicating a complete reaction between $KNbO_3$ and $BaTiO_3$.

The lattice parameters were calculated according to Bragg's law, as $a = b = 3.992$ Å, $c = 4.036$ Å for the pure $BaTiO_3$, $a = b = 3.989$ Å, $c = 4.017$ Å for the doped $BaTiO_3$ (assuming tetragonal phase).

3.3 DSC The DSC results are used to determine the phase transition temperatures. For the pure $BaTiO_3$, transition temperatures for orthorhombic-to-tetragonal transition are 12.9 and 3.4 °C on a heating and cooling trend, respectively and 125.4 °C and 121.3 °C for the tetragonal-to-

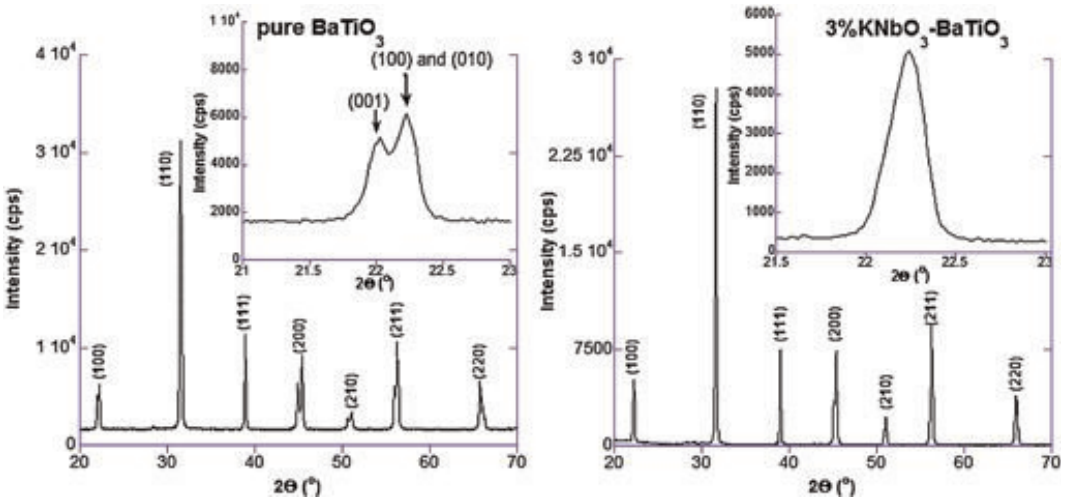

Figure 2 X-ray diffraction spectra for pure (left) and 3%$KNbO_3$ doped (right) $BaTiO_3$ at room temperature. The insets are zoom in {100} peaks. They show either splitting or unsymmetrical characteristic of the {100} peaks, indicating either a tetragonal or an orthorhombic phase, or the coexistence of both phases.

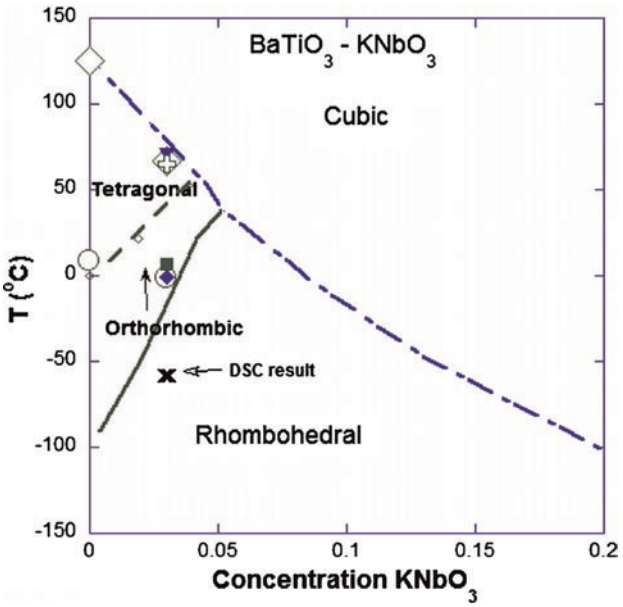

Figure 3 Phase diagram of the $KNbO_3$-$BaTiO_3$ system [6]. Transition temperatures for the corresponding transformations obtained via different methods in the present study have been incorporated as comparison. The hollow dots and hollow diamonds represent the results obtained from DSC tests (the cross represents the rhombohedral-to-orthorhombic transition); the solid triangle and solid square represent those obtained via dielectric measurements; and hollow cross and solid diamond represent transition temperatures obtained from viscoelastic measurements by BVS.

cubic transition on a heating and cooling trend, respectively. For the 3%$KNbO_3$ doped $BaTiO_3$, transition temperatures are 4.77 and −8.96 °C for the orthorhombic-to-tetragonal transition in heating and cooling, respectively, and 72.7 °C and 63.8 °C for the tetragonal-to-cubic transition in heating and cooling, respectively. A hump in heat capacity was observed in the vicinity of −56 °C, corresponding to the rhombohedral-to-orthorhombic transition. However, this hump is only on the order of one-tenth of the magnitude of the humps corresponding to the orthorhombic-to-tetragonal and tetragonal-to-cubic transformations. Given the existence of hysteresis in a first order phase transition, the transition temperature is expressed in the phase diagram as the average of the transformation temperatures, i.e., the peak temperatures of the transformation, during a heating and a cooling trend. The transition temperatures of the ''as-prepared'' samples in the present study have been compared with the published data of the $KNbO_3$-$BaTiO_3$ phase diagram by Bratton [6], as shown in Fig. 3. In that study, the transition temperatures were obtained from maximums on the dielectric constant-temperature curves [6].

3.4 Dielectric measurements Figure 4 shows the temperature dependence of the dielectric constant of 3%$KNbO_3$-$BaTiO_3$ at 10 kHz in both heating and cooling (0.01 °C/s). A hump and a shoulder in dielectric constant are

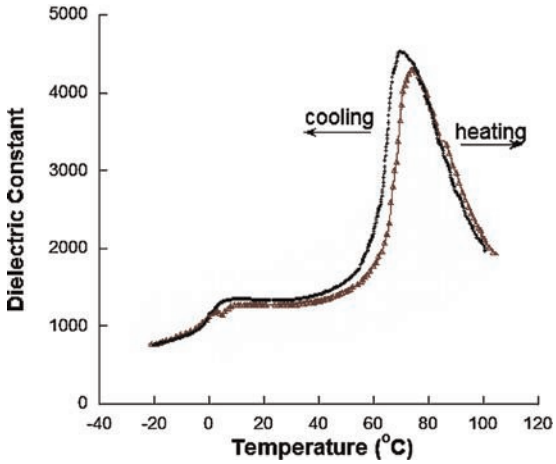

Figure 4 (online color at: www.pss-b.com) Dielectric constant of 3%$KNbO_3$-$BaTiO_3$ as a function of temperature in both heating (right peak) and cooling (left peak) (0.01 °C/s). A frequency of 10 kHz was used.

seen near 70 and 5 °C, which correspond to tetragonal-to-cubic and tetragonal-to-orthorhombic transformations, respectively.

Frequency dependence of the dielectric constant is shown in Fig. 5. Tests were performed in cooling with a rate of 0.01 °C/s. Frequencies of 10^3, 10^4, and 10^5 Hz were used. The magnitude of the dielectric constant in the vicinity of the transformations increases with the inverse of frequency.

3.5 BVS Figure 6 shows elastic modulus $|E^*|$ (absolute value of E^*; a star symbol represents the modulus as a complex number in which the phase represents the damping. The same meaning applies to G^* and K^* in later text) and viscoelastic damping tanδ during heating and cooling of the doped $BaTiO_3$ passing through the orthorhombic-to-tetragonal and tetragonal-to-cubic transformations in both

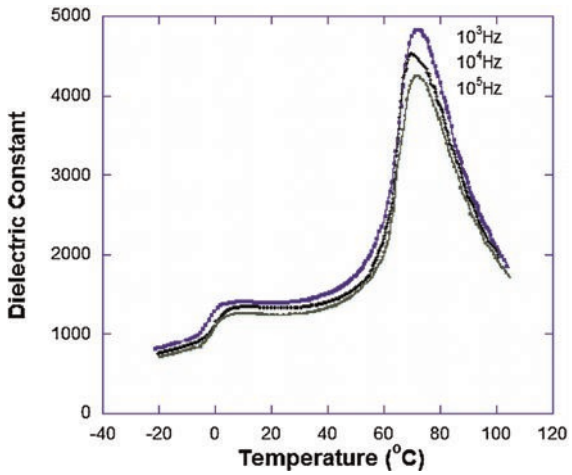

Figure 5 Frequency dependence of dielectric constant of 3%$KNbO_3$-$BaTiO_3$. A thermal rate of −0.01 °C/s was maintained during measurements.

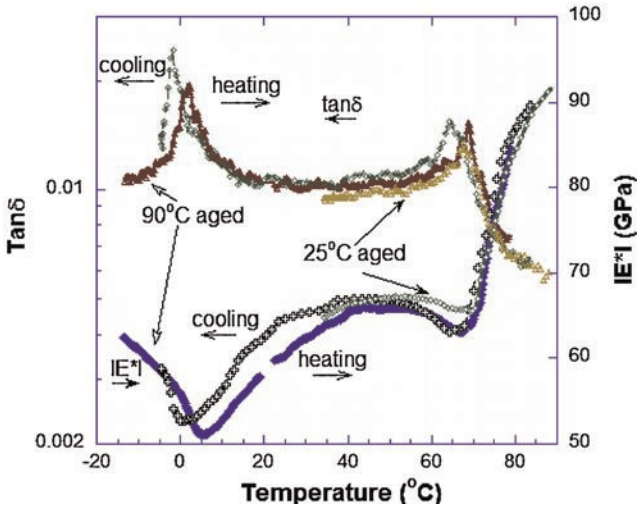

Figure 6 (online color at: www.pss-b.com) Mechanical loss (tanδ) and Young's modulus ($|E^*|$) of 3%$KNbO_3$-$BaTiO_3$ ceramic at 10 Hz excitation frequency. A thermal rate of 0.025 °C/s was applied. The sample was fully rejuvenated above the Curie point prior to test. Mechanical behavior after aging at ambient temperature has been provided as for comparison.

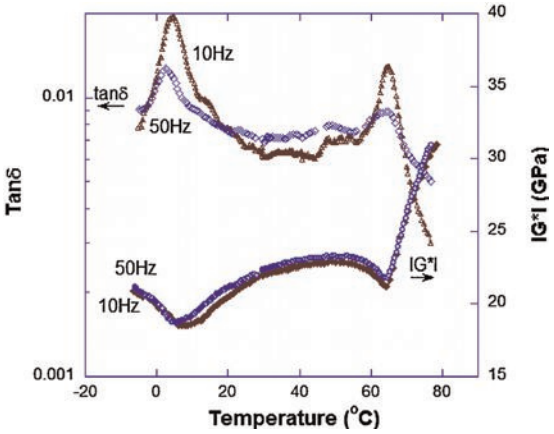

Figure 8 (online color at: www.pss-b.com) Mechanical loss (tanδ) and shear modulus ($|G^*|$) of 3%$KNbO_3$-$BaTiO_3$ ceramic at 10 and 100 Hz excitation frequencies during heating. A thermal rate of 0.05 °C/s was applied.

heating and cooling. An excitation frequency of 10 Hz and a constant temperature ramping rate of 0.025 °C/s were applied. Both transformations are first order, and the mechanical damping during the transformations increases its magnitude with increasing thermal rate and decreasing excitation frequency. The frequency dependence (10, 50, 100 Hz) is shown in Fig. 7. The ramping rate applied was 0.05 °C/s. All these scans were done in heating. The sample was held above the Curie point for a long enough time for rejuvenation prior to the thermal scans. Comparison of Fig. 6 and Fig. 7 provides the dependence of mechanical loss on temperature ramping rate during transformations. The transformations span about 5 °C at half maximum; the higher the temperature ramping rate, the broader the range of temperature for transformations.

A typical mechanical behavior in torsion during heating is shown in Fig. 8. A thermal rate of 0.05 °C/s was applied. Mechanical loss is relatively lower than in bending under the same experimental conditions. Such a difference can be attributed to the volumetric change, in addition to the shape change, of the specimen in bending.

According to Ref. [4], a lower excitation frequency with a more uniform temperature will result in more modulus softening in the vicinity of the transformation. A 0.1 Hz excitation frequency and a slow temperature ramp of 0.005 °C/s were applied to study how much softening can be achieved during transformations. Figure 9 shows the

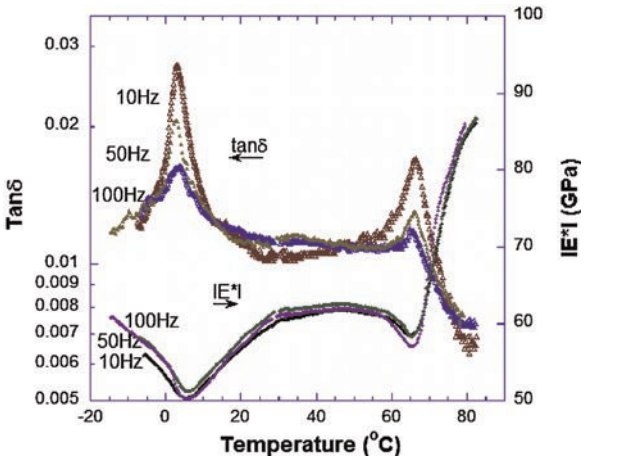

Figure 7 (online color at: www.pss-b.com) Mechanical loss (tanδ) and Young's modulus ($|E^*|$) of 3%$KNbO_3$-$BaTiO_3$ ceramic at 10, 50, and 100 Hz excitation frequencies during heating. A thermal rate of 0.05 °C/s was applied.

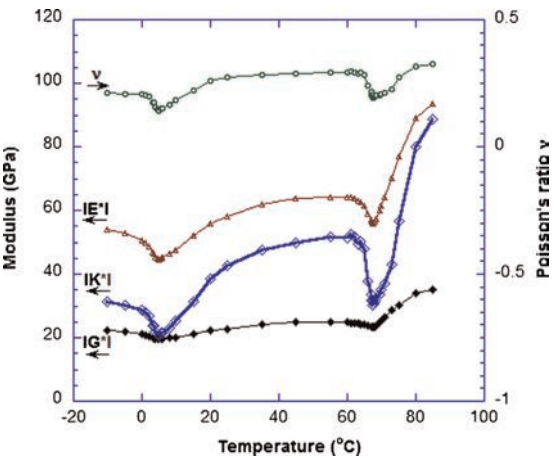

Figure 9 (online color at: www.pss-b.com) Modulus and Poisson's ratio of 3%$KNbO_3$-$BaTiO_3$ ceramic at 0.1 Hz excitation frequencies during heating. A thermal rate of 0.005 °C/s was applied. Damping peaks in the vicinity of the transformations become considerably small due to rate sensitivity in this quasi-isothermal condition.

results of Young's and shear moduli and the corresponding Poisson's ratio and bulk modulus vs. temperature. Only a fraction of the data points is plotted for clarity. The sample was fully rejuvenated above the Curie point prior to the measurement. Because the sample is polycrystalline, the random orientation of the grains leads to the isotropic behavior as a whole. Poisson's ratio and bulk modulus are calculated by applying formulas (1) and (2):

$$\nu = \frac{E}{2G} - 1, \tag{1}$$

$$K = \frac{E}{3(1-2\nu)}. \tag{2}$$

Bulk modulus has softened by a factor of approximately two in the vicinity of either of the transformations, and the Poisson's ratio exhibited a certain amount of reduction. Young's modulus softens during the transformations; however, the softening is less in magnitude than in the electrical short circuited pure $BaTiO_3$ [4] in the vicinity of the transformation. In the pure material, the transformation is sharper and occurs within a temperature window of 1 °C (Fig. 10).

4 Discussion

4.1 Peak width Transformations in the doped ceramic are manifest as peaks in the mechanical damping, peaks in the heat capacity, softening in the bulk modulus, and reductions in the Poisson's ratio. The transformation temperatures determined by these methods agree with each other and are in reasonable agreement with the phase boundaries of Ref. [6], which were determined based on dielectric constant measurements. A different phase diagram was provided [8] in which it

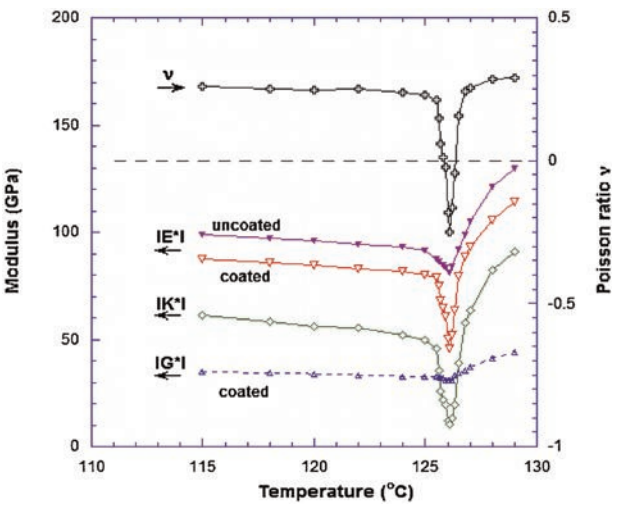

Figure 10 (online color at: www.pss-b.com) Modulus and Poisson's ratio of pure $BaTiO_3$ ceramic at 0.1 Hz excitation frequencies in a quasi-isothermal condition. Adapted from Ref. [4]. Softening in modulus and lowering in Poisson's ratio are shown in the vicinity of the Curie point. Note the difference in temperature scale compared with Fig. 9.

was acknowledged that the drawing was not necessarily to scale. Peaks in internal friction (damping), dielectric constant, and heat capacity were of different width. The transition near 70 °C gave rise to a dielectric peak more than 30 °C wide at half maximum compared with a width of about 5 °C for the damping peak. The transition near 0 °C also gave a damping peak about 5 °C wide but the dielectric peak was shoulder shaped too wide for a quantitative measure of its width. The peak in the dielectric response, though wide (30 °C at half maximum), is not as wide as the dielectric constant peaks reported in Ref. [6], about 100 °C wide at half maximum for 2% and 4% $KNbO_3$-$BaTiO_3$. The phase boundaries provided by Ref. [6] have some uncertainty even though the location of a maximum can be identified with greater precision than the width at half maximum.

The dielectric constant peaks corresponding to three ferroelectric transformations will merge into each other with increasing amount of $KNbO_3$ dopant. In that study, 2%$KNbO_3$-$BaTiO_3$ shows three anomalies in the dielectric constant vs. temperature curve, corresponding to cubic-to-tetragonal, tetragonal-to-orthorhombic, and orthorhombic-to-rhombohedral transitions; for 4%$KNbO_3$-$BaTiO_3$, only two anomalies appear which are claimed to represent the cubic-to-orthorhombic and orthorhombic-to-rhombohedral transitions. As mentioned above, the heat capacity corresponding to the rhombohedral-to-orthorhombic transition is only one-tenth of that of orthorhombic-to-tetragonal transition (heat capacity corresponding to orthorhombic-to-tetragonal transition is about one-third of that of tetragonal-to-cubic transition); from the results of the dielectric measurement in the present study, we have seen that the hump corresponding to the tetragonal-to-cubic transition is much higher than the shoulder corresponding to the orthorhombic-to-tetragonal transition. It seems plausible that the hump corresponding to the rhombohedral-to-orthorhombic transition is much weaker than that of the orthorhombic-to-tetragonal transition, and this makes it almost undetectable on a large scale.

Damping peaks which reveal the transformations in the doped ceramic are broader at half maximum (5 °C) than in the pure $BaTiO_3$ (less than 1 °C). Broadening of the response can result from heterogeneity in the material or in the environment. The role of thermal gradient is evaluated in the following, and found to be insignificant.

4.2 Thermal gradient Experimental procedures aim to reduce the thermal gradients, both along the axial direction and across the cross-section. The apparatus has been updated to achieve better thermal insulation, and the thermal gradient along the axial direction of the sample can be minimized within 0.2 °C. A slow thermal rate was applied in order to allow enough time for thermal equilibration throughout the cross-section of the sample. The time constant for thermal diffusion is given as follows [9]:

$$\tau = \frac{\rho C_p d^2}{4k}, \tag{3}$$

in which τ, d, k, C_p, *and* ρ represent the thermal diffusivity time constant, the depth of penetration of heat in time, the thermal conductivity, the heat capacity, and the mass density, respectively. Given thermal conductivity of 4.7 W/(mK) [10], heat capacity of approximately 200 J/(K kg) for the sample being studied during the phase transformation (heat capacity of the 3%$KNbO_3$-$BaTiO_3$ is about one-third of pure $BaTiO_3$), and a mass density of 5.38 g/cm^3, the thermal diffusion was about 1.7 mm^2 s^{-1}. For a cross-section of 1.68 mm^2, heat transfer could be completed within 0.99 s. When a thermal rate of 0.005 °C/s is applied, the thermal gradient in the cross-section can be neglected.

Thermal gradient caused by thermoelastic effects can be reduced to a negligible level by applying a small excitation strain. For the present study, an excitation strain with the level of approximately 10^{-5} was applied, which corresponds to a thermal gradient about 0.06 °C due to thermoelastic coupling according to Eq. (4):

$$\Delta T = -\frac{\alpha E \varepsilon T}{C_V}, \tag{4}$$

in which E is Young's modulus (65 GPa), C_V is heat capacity per unit volume (1.076 J/K m^3), and α is the linear coefficient of thermal expansion (10^{-4}/ °C in the vicinity of the transformation). In summary, thermal gradient is insufficient to account for the observed width of the transition.

4.3 Material heterogeneity Material heterogeneity can cause the transformation to appear broader [1]; if there is a range of compositions on a fine scale, there will also be a range of transformation temperatures. Doped ceramic grain has the so-called "core-shell" structure [11]: the grain core remains pure, but the dopant content increases toward the grain boundary, and thus gives rise to a distribution of transition temperature. Such a fact is considered as due to the partial intragranular diffusion of dopant. Repeated grinding and sintering procedure would reduce this effect.

To appreciate this effect, the constrained negative stiffness theory could be applied: a grain is decomposed into core (shell 0), shell 1, shell 2, shell 3, ... shell n, shell $n+1$,... from the center to the grain boundary. The core is pure $BaTiO_3$, and the concentration of dopant in each shell increases with the shell number. Doped $BaTiO_3$ has a lower Curie point than the pure $BaTiO_3$, and the more concentration of dopant, the lower the Curie point. In either heating or cooling, when shell n is undergoing transformation, shell $n+1$ is still in the parent phase. The modulus of the transforming part (shell n) is lower, and could become negative in the light of Landau's theory; while the untransformed part (shell $n+1$) is stiffer. Such a modulus configuration composed of shell n and $n+1$ would give rise to the constrained negative stiffness effect, i.e., damping and modulus anomalies. The transformation temperature has a distribution from the center toward the grain boundary, and so do the moduli of the shells. Distributed constrained negative stiffness would give rise to a broad hump in the modulus curve rather than a sharp peak. Such a broad hump could thus reduce the apparent modulus softening in the vicinity of the transformation temperature(s).

4.4 Contributions for modulus softening The mechanical loss spectrum obtained during a first order phase transformation can be decomposed into three terms [12]:

$$\tan\delta = \tan\delta_{\text{transient}} + \tan\delta_{\text{PT}} + \tan\delta_{\text{intrinsic}}.$$

The first term is the transient component of the total mechanical loss, and is proportional to thermal rate and the inverse of excitation frequency. The second term represents the contribution from the phase transformation itself, and is independent of thermal rate applied. The third term is the intrinsic component, which comes from the fractional contribution of both parent and new phases during the transformation. In an isothermal condition, the first term vanishes, and the second and third terms become the only contribution to the mechanical loss spectrum.

In the same way, the modulus defect (softening) can be decomposed into three terms as follows:

$$\Delta E = \Delta E_{\text{transient}} + \Delta E_{\text{PT}} + \Delta E_{\text{intrinsic}}.$$

The first transient term is thus proportional to thermal rate and excitation frequency. A fast thermal rate and a low frequency will promote the phase interface motion [13], giving rise to more softening. However, too fast a thermal rate would lead to a significant thermal gradient along the cross-section of the sample, which will reduce the apparent modulus softening during the transformation. Moreover, a high enough thermal rate would give rise to a sigmoid-shaped anomaly in the modulus versus temperature curve in the vicinity of the transformation due to the effect of constrained negative stiffness elements by surrounding grains which have passed the transition temperature [14]. The transient term will vanish in an isothermal condition. The second term, i.e., the contribution from the phase transition itself, comes from the phonon mode freezing [15] which is independent of thermal rate. Specifically, this softening is attributed to the coupling between spontaneous strain and the order parameter, which in barium titanate refers to certain tilt angles of the oxygen octahedron with respect to reference coordinate axis. When the restoring force opposing the tilting of octahedron becomes too small to recover the tilt at a particular spontaneous strain level, the system becomes soft or unstable. The doped $BaTiO_3$ has reduced unit cell volume compared with the pure $BaTiO_3$ (about a factor of 1.006) at room temperature, and is closer to the unit cell volume in the cubic phase. These will lead to reduced spontaneous electric polarization magnitude and spontaneous strain level; hence less coupling effect is involved during the transformation which gives rise to less softening in the modulus. Moreover, the tetragonal distortion from cubic is less in the doped material than in pure barium

titanate: the unit cell ratios are $c/a = 1.01$ in pure barium titanate and for example, $c/a = 1.001$ in 2%$KNbO_3$-$BaTiO_3$ [6].

The third term is the minor contribution as it only provides the baseline for modulus change during the transformation, and will not account for the reduced modulus softening observed in the doped than in the pure $BaTiO_3$.

4.5 Defect polarization effect The mechanical behavior of the doped $BaTiO_3$ after aging 20 h at ambient temperature has been provided in Fig. 6. Compared with the behavior of rejuvenated sample above the Curie point, modulus softening is less prominent in the vicinity of the transformation. Such an effect can be attributed to the oxygen vacancy contribution described as follows.

Oxygen vacancies (OVs) play an important role in the behavior of barium titanate. A schematic oxygen octahedron in tetragonal $BaTiO_3$ is shown in Fig. 11. Spontaneous polarization $\mathbf{P}_s$ exists below the Curie point. Impurities, such as Al^{3+}, Fe^{3+}, Sr^{2+}, will replace Ti^{4+}, and form defect dipoles with OVs. According to the mechanism of symmetry-conforming property of point defects [16], OV can occupy either of A (or B) or C sites of the oxygen octahedron with identical conditional probabilities above the Curie point since A (or B) and C sites have the same distances from the center. Below the Curie point, OV tends to migrate to and accumulate at C sites, which are closer to the center of octahedron, from A (or B) sites during aging. Therefore, defect dipole moment $\mathbf{P}_d$ exists in specimens aged below the Curie point but not above. During the transformation, $\mathbf{P}_s$ appears (or disappears) immediately after passing through the Curie point; however, $\mathbf{P}_d$ will not disappear immediately as it requires time to allow OVs to distribute into a new configuration. The existence of $\mathbf{P}_d$ can account for the divergence in mechanical behavior in the vicinity of the transformation. It can be regarded as a portion of the material is not transforming while the remaining parts are undergoing the phase transition, and hence reduce the apparent modulus softening.

In most cases, full rejuvenation cannot always be completed considering the time factor, and sample is usually partial rejuvenated [17]. The minor divergence in modulus behaviors over thermal cycles could be attributed to this oxygen vacancy effect.

4.6 Poisson's ratio and softening of bulk modulus In polycrystalline $BaTiO_3$, both pure and doped, the bulk modulus softens more than the shear modulus, corresponding to minima in the Poisson's ratio. While pure $BaTiO_3$ is auxetic (Poisson's ratio to –0.25) in the vicinity of transfromation temperatures, the present doped $BaTiO_3$ exhibits broad minima in Poisson's ratio no lower than about +0.15. The Landau theory predicts softening of moduli (the bulk modulus in the present case) to zero corresponding to Poisson's ratio approaching –1. The difference is attributed to heterogeneity of composition on a fine scale giving rise to a range of transition temperatures. Transformation of small regions at a given temperature in this case is insufficient to bring about large softening of the bulk modulus or Poisson's ratio approaching –1.

5 Conclusion Viscoelastic loss and modulus of 3%$KNbO_3$-$BaTiO_3$ via broadband viscoelastic spectroscopy over a range of temperature passing through both the orthorhombic-to-tetragonal and tetragonal-to-cubic phase transformations disclose peaks in damping and minima in bulk modulus and Poisson's ratio. Transition temperatures of both transformations shifted to lower temperatures. Damping peaks vs. temperature are broader (5 °C wide at half maximum) than pure $BaTiO_3$ (less than 1 °C wide). Damping peaks are sharper than peaks in dielectric constant or heat capacity. Softening in bulk modulus and lowering in Poisson's ratio occur in the vicinity of the transformations, but have a smaller magnitude than in pure $BaTiO_3$. Reduced coupling effect between spontaneous strain and order parameters and the heterogeneous composition distribution, i.e., so called "core-shell" structure are considered to be responsible for the width and reduced magnitude of effects in doped vs. pure ceramic.

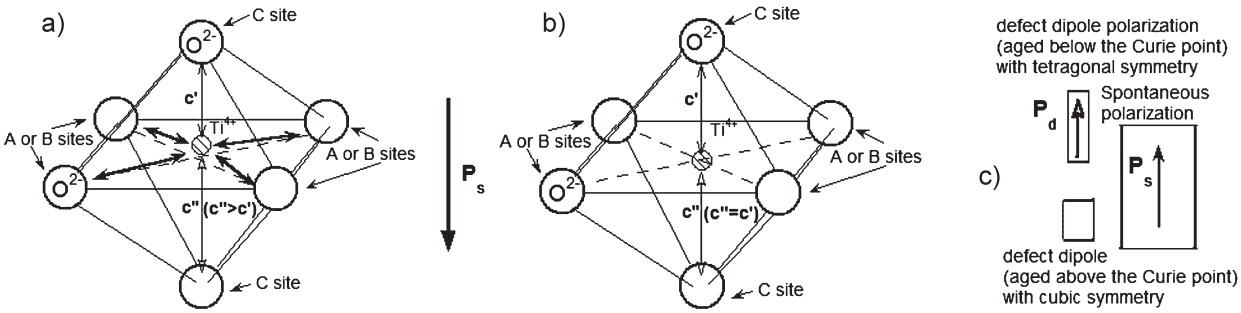

Figure 11 (a) Oxygen octahedron in tetragonal barium titanate. O^{2-} has two kinds of non-equivalent sites A or B and C. In the tetragonal phase, distance between Ti^{4+} and A (B) and C sites are not equal. (b) In cubic phase, the distance between Ti^{4+} and A or B and C sites are the same. (c) An 180° domain in barium titanate. After enough time of aging at room temperature, $\mathbf{P}_d$ is generated. After rejuvanation above the Curie point, $\mathbf{P}_d$ is not generated shortly after temperature is cooling through the Curie point, i.e., without aging at tetragonal phase, and defects possess cubic symmetry, therefore no $\mathbf{P}_d$.

References

[1] Y. Avrahami and H. L. Tuller, J. Electroceram. **13**, 463–469 (2004).
[2] L. D. Landau, in: Collected Papers of L. D. Landau, edited by D. Ter Taar (Gordon and Breach/Pergamon, New York, 1965).
[3] T. Jaglinski, D. Kochmann, D. S. Stone, and R. S. Lakes, Science **315**, 620–622 (2007).
[4] L. Dong, D. S. Stone, and R. S. Lakes, Philos. Mag. Lett. **90**, 23–33 (2010).
[5] R. S. Lakes, T. Lee, A. Berise, and Y. C. Wang, Nature **410**, 565–567 (2001).
[6] R. J. Bratton and T. Y. Tien, J. Am. Ceram. Soc. **50**, 90–93 (1967).
[7] F. Kulcsar, J. Am. Ceram. Soc. **39**, 13–17 (1956).
[8] Y. Avrahami and H. L. Tuller, US Patent No.: US 6,526,833 B1 (2003).
[9] J. F. Ready, Interaction of high-power laser radiation with material, in: Industrial Application of Lasers, Second edition (Academic Press, New York, 1997).
[10] A. J. H. Mante and J. Volger, Phys. Lett. A **24**, 139–140 (1967).
[11] D. Hennings and G. Rosenstein, J. Am. Ceram. Soc. **67**, 249–254 (1984).
[12] R. B. Perez Saez, V. Recarte, M. L. No, and J. S. Juan, Phys. Rev. B **57**, 5684–5692 (1998).
[13] J. X. Zhang, P. C. W. Fung, and W. G. Zeng, Phys. Rev. B **52**, 268–277 (1995).
[14] T. Jaglinski, P. Frascone, B. Moore, D. S. Stone, and R. S. Lakes, Philos. Mag. **86**, 4285–4303 (2006).
[15] R. Blinc and B. Zeks, Soft modes in ferroelectrics and antiferroelectrics (North-Holland Publ. Co., Amsterdam, Oxford, 1974).
[16] X. B. Ren, Nature Mater. **3**, 91–94 (2004).
[17] V. Mueller and Y. Shchur, Europhys. Lett. **65**, 137–141 (2004).

